# Experimental studies on fast-ion transport by Alfvén wave avalanches on the National Spherical Torus Experiment[a)]

M. Podestà,[1,b)] W. W. Heidbrink,[1] D. Liu,[1] E. Ruskov,[1] R. E. Bell,[2] D. S. Darrow,[2] E. D. Fredrickson,[2] N. N. Gorelenkov,[2] G. J. Kramer,[2] B. P. LeBlanc,[2] S. S. Medley,[2] A. L. Roquemore,[2] N. A. Crocker,[3] S. Kubota,[3] and H. Yuh[4]
[1]*Department of Physics and Astronomy, University of California, Irvine, California 92697, USA*
[2]*Princeton Plasma Physics Laboratory, Princeton, New Jersey 08543, USA*
[3]*University of California Los Angeles, California 90095, USA*
[4]*Nova Photonics, Princeton, New Jersey 08543, USA*

(Received 10 December 2008; accepted 22 January 2009; published online 13 March 2009)

Fast-ion transport induced by Alfvén eigenmodes (AEs) is studied in beam-heated plasmas on the National Spherical Torus Experiment [Ono *et al.*, Nucl. Fusion **40**, 557 (2000)] through space, time, and energy resolved measurements of the fast-ion population. Fast-ion losses associated with multiple toroidicity-induced AEs (TAEs), which interact nonlinearly and terminate in *avalanches*, are characterized. A depletion of the energy range $>20$ keV, leading to sudden drops of up to 40% in the neutron rate over 1 ms, is observed over a broad spatial range. It is shown that avalanches lead to a relaxation of the fast-ion profile, which in turn reduces the drive for the instabilities. The measured radial eigenmode structure and frequency of TAEs are compared with the predictions from a linear magnetohydrodynamics stability code. The partial disagreement suggests that nonlinearities may compromise a direct comparison between experiment and linear theory. © *2009 American Institute of Physics*. [DOI: 10.1063/1.3080724]

## I. INTRODUCTION

The dynamics of fast-ion populations plays a primary role in several aspects of magnetically confined plasmas.[1] Beams of fast neutral particles are commonly used to heat the plasma and for noninductive sustainment of the plasma current. Radio-frequency (rf) waves are also used to create high-energy populations for similar purposes. Regarding magnetohydrodynamic instabilities, fast ions can provide a stabilizing effect, e.g., for internal kink modes.[2] Fast ions are finally responsible for the fusion reactions occurring in magnetically confined plasmas. Beside these beneficial effects, unconfined fast ions can damage in-vessel components such as limiters, rf antennas, or the vessel wall.[3] These negative aspects will acquire even stronger relevance for reactors such as ITER, where alpha particles originate from fusion reactions with an energy of 3.5 MeV, much higher than the thermal energy of ions and electrons. Understanding fast-ion dynamics is therefore a primary task for near-term fusion studies.[4] Closely related to that is the possibility of predicting fast-ion dynamics through theoretical studies and reliable models. Finally, affecting fast-ion dynamics through the injection of rf waves or neutral beams (NBs) may open new avenues to control the behavior of a fusion reactor.

Waves in the Alfvén frequency range are well known for their potential interaction with a fast-ion population. Experimentally, loss and redistribution in both the real and the velocity space are observed in beam-heated plasmas on several devices (cf. Refs. 1 and 4 and references therein). Of particular interest are modes that can coalesce nonlinearly, until the associated resonances overlap in phase space.[5,6] In this case, extended regions of the fast-ion distribution function can provide free energy to sustain the modes' growth. The resulting stochastization of phase space leads to greatly enhanced losses and redistribution, compared to the case of multiple, but noninteracting modes. In this paper, we focus on fast-ion dynamics associated with toroidicity-induced Alfvén eigenmodes (TAEs) and their nonlinear evolution in *avalanches*.[7] The latter manifest as a fast ($\sim 1$ ms) frequency downchirp involving multiple modes, often associated with a prompt decrease in the neutron rate, indicating loss or redistribution of energetic ions. Measurements presented herein are performed on the National Spherical Torus Experiment (NSTX),[8] where NB injection provides the main source of additional heating. Due to the high ratio between beam-ion and Alfvén velocities, a large variety of Alfvénic instabilities are destabilized,[9] providing a suitable environment for their experimental investigation.

NSTX is a small aspect ratio device, with major and minor radii of $R_0=0.8$ m and $a=0.65$ m (aspect ratio $R/a \approx 1.3$). The magnetic field is $3.5 \rightarrow 5.5$ kG for a pulse duration of $\sim 1$ s. The density and temperature are $n_e=1 \rightarrow 10 \times 10^{19}$ m$^{-3}$ and $T_i \approx T_e \leq 1.5$ keV (subscripts $e$ and $i$ refer to electrons and ions, respectively). Up to 7 MW of NB power is injected from three NB sources named A, B, and C, with tangency radii of 69, 59, and 49 cm, respectively. The maximum acceleration voltage is 95 kV, with deuterium being the standard injected species. The velocity of fast ions resulting from charge exchange of the injected neutrals is up to five times the Alfvén velocity $v_A$. Several resonant mechanisms are thus accessible to destabilize waves in the Alfvén frequency range.

Figure 1(a) shows a spectrogram from Mirnov coils

[a)]Paper GI1 1, Bull. Am. Phys. Soc. **53**, 78 (2008).
[b)]Invited speaker. Electronic mail: mpodesta@pppl.gov.

 

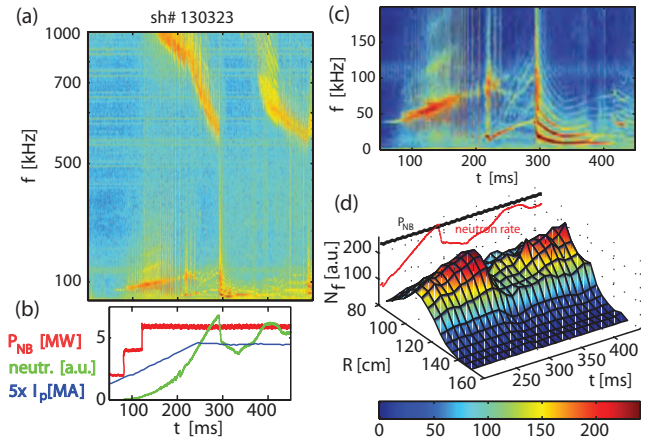


FIG. 1. (Color) [(a)–(c)] Spectrograms of magnetic fluctuations during NB injection on NSTX. (b) Time traces of injected NB power (red), neutron rate (green), and plasma current (blue). (d) Fast-ion profile evolution measured via FIDA spectroscopy.

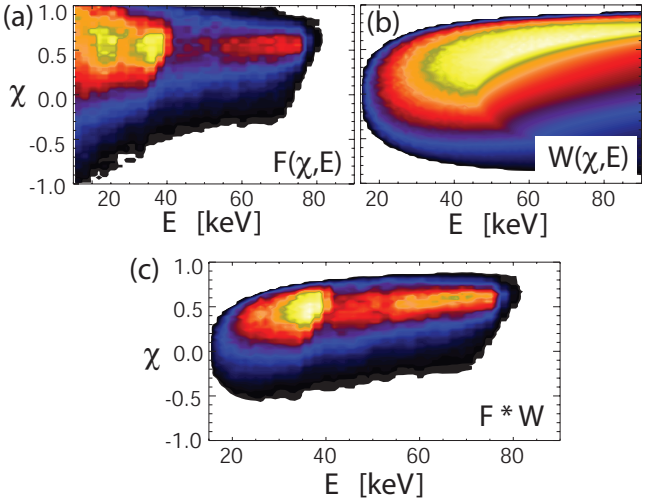


FIG. 2. (Color) (a) Fast-ion distribution $F$ calculated by TRANSP (injection energy is 75 keV). (b) FIDA response function $W$ obtained from a simulation code. (c) Convolution $F*W$, determining the measured FIDA signal.

(shot 130323) to introduce the variety of modes commonly observed in NSTX beam-heated discharges. For that discharge, 6 MW of NB power was injected [Fig. 1(b)] into a deuterium plasma. The flat-top phase, starting at $t \approx 200$ ms, is characterized by a plasma current $I_p = 0.9$ MA. For practical purposes, three spectral regions are identified.[10,11] Low-frequency, kinklike modes are destabilized at frequencies $f \leq 50$ kHz, see Fig. 1(c). In the same range can be found beta-induced acoustic Alfvén eigenmodes[12,13] and energetic-particle modes (EPMs). The range of $50 \leq f \leq 200$ kHz typically corresponds to the TAE range. Finally, for $f > 200$ kHz modes pertaining to higher order Alfvén gaps are observed.[14,15] A first idea of the effect of instabilities on fast ions can be inferred from the volume-averaged neutron rate [Fig. 1(b)]. Before $t \approx 200$ ms, i.e., during the current ramp-up phase, quasiperiodic bursts of EPMs occur, leading to prompt drops of the neutron rate up to 15%. Then, a low-frequency kinklike mode appears at $t \approx 300$ ms, accompanied by a strong, long-lasting decrease in the neutron rate. The dramatic effects on the fast-ion population can be appreciated from Fig. 1(d), showing the evolution of the fast-ion density profile as measured by fast-ion D-alpha (FIDA) spectroscopy (see Sec. II).

The paper is organized as follows. The diagnostics available on NSTX for fast-ion studies are described in Sec. II. Section III presents the experimental results on fast-ion dynamics during TAE avalanches. The approach to modeling the observed losses is discussed in Sec. IV. Finally, the results are summarized in Sec. V.

## II. THE NSTX FAST-ION DIAGNOSTICS

The main diagnostics utilized throughout this paper are FIDA systems,[16,17] which became available on NSTX in 2008.[18] They are based on active charge-exchange recombination spectroscopy. The measured FIDA signal is given by $s = s_f + B$, where $B$ indicates background light and $s_f$ the fast-ion signal, associated with fast ions that recombine with the injected neutrals. After recombination, a fraction of these *re-neutrals* will eventually undergo plasma collisions and be in an excited state. The signal $s_f$ originates from photons emitted after a $3 \rightarrow 2$ transition between excited states. The corresponding wavelength range is centered about the $D_\alpha$ (or Balmer-alpha) emission line at 656.1 nm. For recombining fast ions with sufficiently high energy, the Doppler-shifted emission can be separated from the (dominant) cold $D_\alpha$ light, thus making the information on the fast-ion population available. Referring to Fig. 2, $s_f$ can be expressed as

$$s_f(E_\lambda) \equiv \int\int W F_f dE d\chi, \tag{1}$$

where $E_\lambda$ is the energy calculated from the observed wavelength $\lambda$ through the Doppler shift formula. $F_f(E,\chi)$ is the local fast-ion distribution, with $E$ and $\chi = v_{f,\parallel}/v_f$ the energy and pitch variables ($v_f$ is the fast-ion velocity and $v_{f,\parallel}$ its component along the magnetic field). The *response function* $W(E,\chi)$ accounts for the effective averaging over the phase space, intrinsic to the method,[17] for the specific viewing and beam geometry and for the charge-exchange rate. In practice, the integrated fast-ion signal is approximated as

$$\int_{\Delta E_\lambda} s_f dE_\lambda \propto N_f N_b \langle \sigma_{cx} \vec{v} \rangle, \tag{2}$$

from which the *FIDA density* $N_f$ is obtained from the experimental data. The integration range $\Delta E_\lambda$ in Eq. (2) corresponds to the expected fast-ion energy range.

The use of Eqs. (1) and (2) requires two important remarks for a correct interpretation of the experimental results. First, each channel samples a limited portion in velocity space, therefore the assumption that $N_f$ is representative of the actual fast-ion density must be verified. This can be done by comparing the experimental results with the output of a dedicated numerical code, simulating the response of FIDA under different conditions. Second, Eq. (1) involves a

convolution over energy and pitch, resulting in (i) a reduction in the overall velocity-space resolution and (ii) a loss of a one-to-one correspondence between original fast-ion energy $E$ and *observed* energy $E_\lambda$. Again, the comparison with simulations can be used to untangle the spectral information contained in the data.

Two complementary instruments are operational on NSTX, namely a spectrometer (s-FIDA) and a filter-based (f-FIDA) system.[18] s-FIDA has 16 radial channels, measuring the whole spectrum in the $D_\alpha$ range. It provides data with spatial and spectral resolution of 5 cm and 10 keV and temporal resolution of 10 ms. f-FIDA has three radial channels at $R=100$, 120, and 140 cm. It integrates the $D_\alpha$ light over a convenient spectral range through a bandpass filter. This improves the achievable temporal resolution up to 20 $\mu$s, at the expense of the energy resolution. An acceptable signal-to-noise ratio is achieved with sampling frequencies of 50 kHz, limited by statistical photon noise. Note that for most NSTX discharges the data from $R=140$ cm are dominated by direct beam-emission light and is not representative of the behavior of confined fast ions. Each *channel* of the two systems is composed by two paired views spaced toroidally by 30°, intercepting/missing the NB at the same radial location. The net FIDA signal is the difference between these *active* and *passive* views.[19] This scheme allows one to remove the background signal not associated with fast ions, e.g., from cold $D_\alpha$, bremsstrahlung, and impurity emission.[18]

For practical purposes, a least-squares fit with a known function is used in the following to derive properties of the fast-ion density profile from s-FIDA, such as its maximum and full width at half maximum. The errors in the above mentioned quantities are also estimated from the fit. Empirically, a modified Gaussian is a suitable choice as fitting function, with an additional parameter accounting for the *squareness* of the profile. For the data presented hereafter, the innermost channels ($R\lesssim 95$ cm) are usually excluded from the fit because of the poor signal-to-noise ratio due to the strong attenuation of the injected beam and the low NB power.

In addition to the FIDA systems, information on the fast-ion behavior is gathered from the volume-averaged neutron rate $S_n$, which is mostly determined on NSTX by beam-plasma reactions. $S_n$ depends strongly on the density of high-energy ($\geq$60 keV), centrally confined fast ions due to the energy dependence of the fusion cross section and to the higher density of target ions in the plasma core. Other fast-ion diagnostics available on NSTX include neutral particle analyzers[20–23] (NPAs) and a scintillator-based energetic ion loss probe (sFLIP).[24] Plasma profiles are measured by multipoint Thomson scattering[25] and charge-exchange recombination spectroscopy systems. Plasma density fluctuations are measured through a five-channel reflectometer.[26] Magnetic field fluctuations are measured by Mirnov coils, located close to the vacuum vessel wall at the low-field side. A motional-Stark-effect diagnostic,[27] requiring the injection of NB source A at 90 kV, is also available to document the evolution of the safety factor profile $q(R)$.

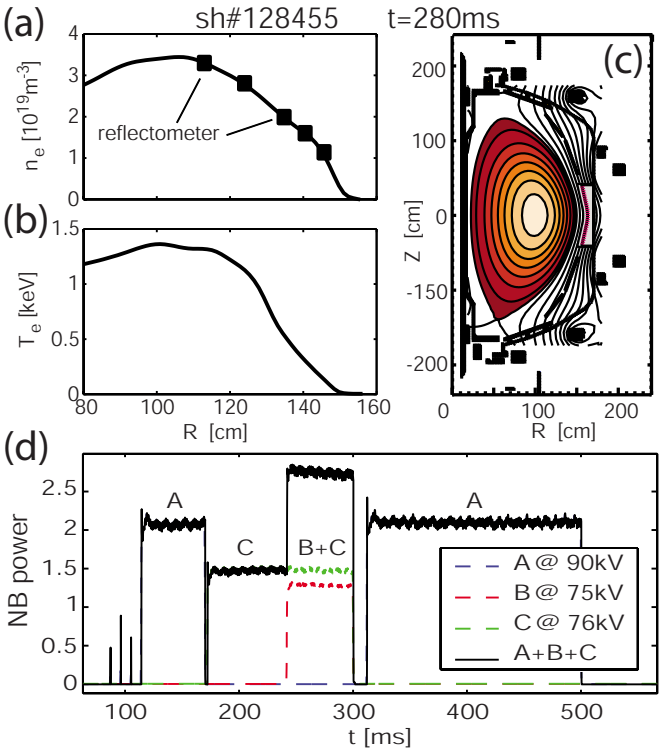


FIG. 3. (Color online) [(a) and (b)] Density and electron temperature profiles. Symbols refer to the measurement locations of a multichannel reflectometer. (c) Magnetic flux surfaces. (d) NB power waveform.

## III. EXPERIMENTAL RESULTS

A suitable scenario has been achieved on NSTX to study TAEs and TAE avalanches. The target is a helium $L$-mode plasma with peak density $n_e\sim 4\times 10^{19}$ m$^{-3}$ and $T_i\approx T_e \leq 1.3$ keV [Figs. 3(a) and 3(b)]. The toroidal field and Alfvén velocity are 0.45 T and $1.2\times 10^6$ m/s on axis. The magnetic configuration has a lower single null point, with elongation of 2.1 and triangularity of 0.46 [Fig. 3(c)]. Having a higher $L\rightarrow H$ transition threshold, helium plasmas help maintain $L$-mode discharge conditions. This is preferred because of the availability of reflectometer data over a good portion of the minor radius [Fig. 3(a)], unlike for $H$-mode plasmas. Auxiliary heating is provided by $1.5\rightarrow 2.7$ MW of NB power [Fig. 3(d)]. The NB power waveform has source A (used for $q$-profile measurements) active before and after the time range of interest, which spans from $t=200$ ms to $t=300$ ms. During this time, the NB power delivered by sources B and C can be varied on a shot-to-shot basis. For the configuration presented herein, quasistationary TAE modes are destabilized when the power exceeds $\approx$2.3 MW. Toroidal mode numbers $n\leq 6$ are observed in the frequency range of 50–200 kHz [Fig. 4(a)]. Slightly above the TAE threshold, i.e., for $P_{\mathrm{NB}}\geq 2.5$ MW, TAE avalanches eventually occur. This is detailed in the inset of Fig. 4(a), where the avalanche appears as a frequency downchirp of 50 kHz over 1 ms which involves all the observed modes. At this time $q\approx 1.5$ on axis, with a minimum value of 1.4 at $R\approx 125$ cm. Typical toroidal rotation frequencies are 30 kHz at the magnetic axis, reduced to $\lesssim$10 kHz at $R=125$ cm.

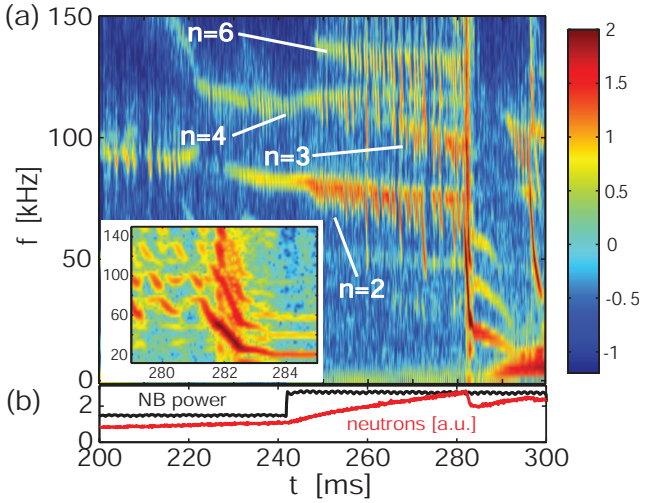


FIG. 4. (Color) (a) Spectrogram of magnetic fluctuations showing the onset of TAE activity after $t=220$ ms, followed by an avalanche at $t\approx 282$ ms, as detailed in the inset. (b) Time traces of NB power (black) and neutron rate (red).

### A. Dynamics of TAE modes

The scenario illustrated in Fig. 4 suggests that avalanches are the results of an increase in the drive for the underlying TAE modes. It is worth noting that nonlinear theories on weakly turbulent systems are able to mimic such behavior.[6] For example, the amplitude of a TAE mode driven unstable by a strong source (such as NB injection) is expected to saturate at different levels, depending on both the source and the damping terms, both of which may evolve in time. Different regimes are possible, including cases characterized by repetitive amplitude bursts and frequency chirps, as observed experimentally. In particular, a chirping frequency may indicate resonance overlap in phase space, consistent with the general picture of multiple avalanching modes. In this framework, the quest for a general threshold condition leading to avalanches should then focus on the dynamics of the precursors, rather than on the avalanche itself. Figure 5(a) shows the amplitude of the modes with $n=2,4,6$, calculated from the spectrogram (Fig. 4). A measure of the bursty behavior of the mode is provided by the deviation of the mode amplitude $\sigma_A$ from its mean value. $\sigma_A$ is calculated over a moving time window of width of 2.5 ms. The amplitudes fluctuate with increasingly large variations in time after the second NB source is switched on at $t=240$ ms [Fig. 5(b)]. Similarly, the frequency evolution is shown in Fig. 5(c) in terms of normalized variation $\sigma_f/f$ to quantify the chirping nature of the modes. In this case, large fluctuations are already observed 20 ms before the avalanche. The details of the amplitude evolution for the $n=2$ mode are shown in Fig. 6. Within the temporal resolution of the Fourier analysis used to calculate the spectrogram, two distinct phases are identified. As source B is turned on, the amplitude increases exponentially with an effective growth rate $\gamma\approx 0.5\times 10^3$ s$^{-1}$, i.e., $\gamma/2\pi f\sim 7\times 10^{-3}$. (As a comparison, the slowing-down time for beam ions is $\approx 30$ ms.) The frequency remains constant. Then, large fluctuations are observed in both amplitude and frequency. The maximum of

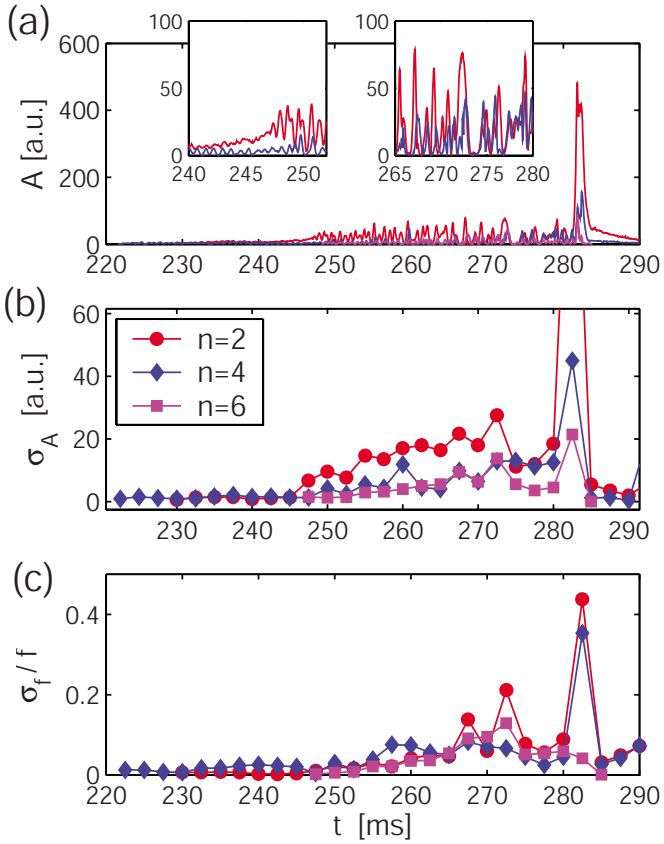


FIG. 5. (Color online) (a) Amplitude of the $n=2,4,6$ modes from Mirnov coils. The insets show a zoomed view at the turn-on of the second NB source and right before the avalanche. (b) Envelope of the amplitude over 2.5 ms time windows. (c) Relative frequency variation.

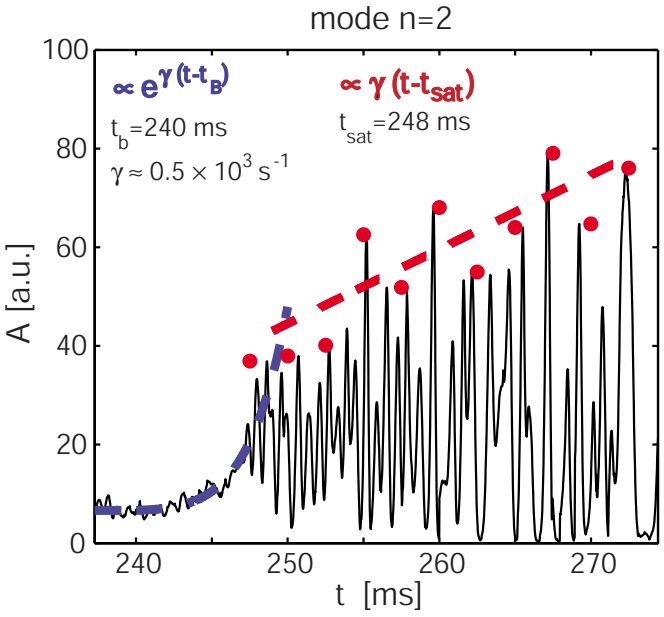


FIG. 6. (Color online) Detail of the amplitude evolution for the $n=2$ mode (see Fig. 5), showing the two intervals corresponding to exponential and linear growth of the maximum amplitude. Thick, dashed lines are the result of a least-squares fit of the maximum amplitude calculated over 2.5 ms time windows.

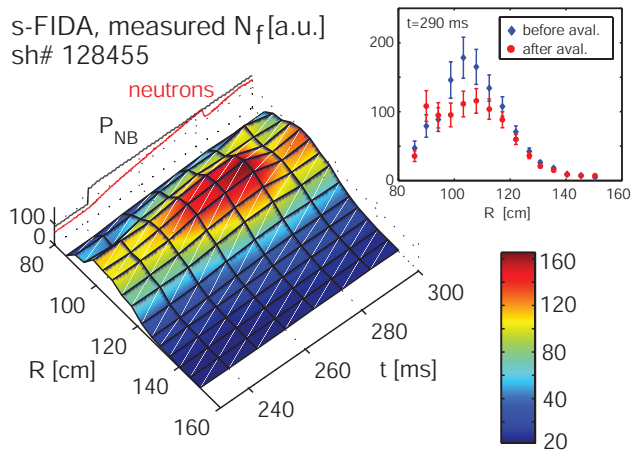


FIG. 7. (Color) Measured evolution of the fast-ion profile. The decrease after $t=280$ ms, following a TAE avalanche, is detailed in the inset.

amplitude fluctuations continues to increase roughly linearly in time, on a time scale comparable with the slowing-down time. As discussed later in this paper, no quantitative information on a threshold in drive and damping terms can be established on a solid basis until the actual relationship between mode structure and signal on magnetic probes is established. A more complete characterization of the dynamics of the TAE avalanche precursors remains therefore an open issue.

### B. Fast-ion dynamics

After an avalanche is triggered, a sudden drop in the neutron rate occurs [Fig. 4(b)]. This correlates with a depletion of the fast-ion profile measured by s-FIDA, as illustrated in Fig. 7. According to the spectra measured by s-FIDA [Fig. 8(a)], the observed decrease in fast-ion density involves a broad energy range above ≈15 keV. However, because FIDA spectra are the result of a convolution and smearing in phase space [cf. Eq. (1) and Fig. 2], their interpretation is not straightforward. Data from FIDA are complemented by measurements from a solid state NPA diagnostic, characterized by a good spectral resolution. The energy spectrum from the central channel aimed at tangency radius of 100 cm is shown in Fig. 8(b). An increase in lost fast-ion signal up to the injection energy is clearly observed after $t=280$ ms. Conversely, the energy and pitch of lost fast ions observed by the sFLIP diagnostic for this discharge extend over a narrow range about the injection energy, but with highly perpendicular velocity.

The relationship between the fractional drop in the volume-averaged neutron rate and the local fast-ion density following an avalanche is shown in Fig. 9(a) for a series of similar shots. The fractional loss from s-FIDA is calculated from the integral of $N_f$ along the radius. Overall, a good agreement between the two quantities is observed, confirming the consistency of FIDA and neutron rate data. Figure 9(b) illustrates the change in the radial gradient of $N_f$, calculated at the position of steepest gradient at the low-field side. The gradient is actually calculated from a fit of the measured profile, as explained in Sec. II. This procedure is justified if

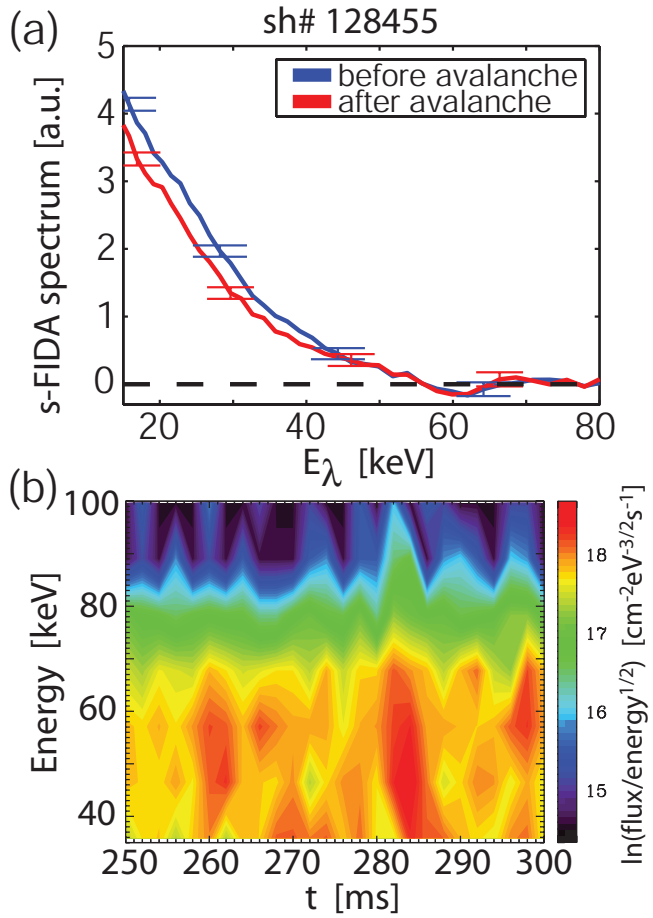


FIG. 8. (Color) (a) Energy spectrum measured by s-FIDA at $R=115$ cm, before and after a TAE avalanche. (b) Energy spectrum of lost fast ions vs time, measured by the ssNPA. Note the increased losses around $t=282$ ms.

the measured profile is smooth, as for the cases considered herein (cf. Fig. 7), especially on the low-field side portion of $N_f(R)$. The difference between the gradient after and before an avalanche indicates that it relaxes to smaller values. In

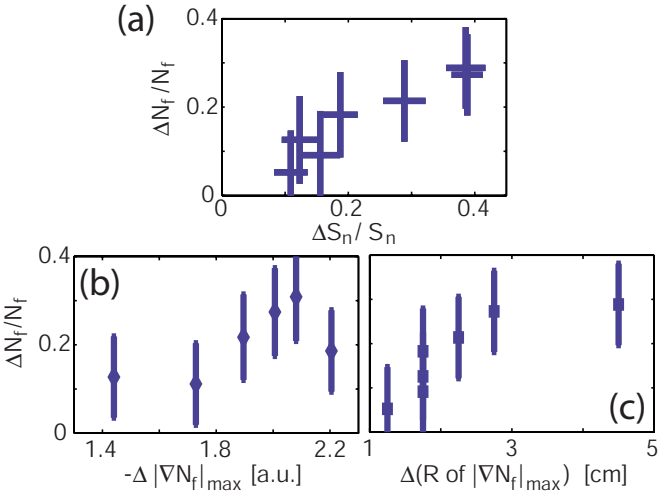


FIG. 9. (Color online) (a) Comparison between the fractional drop in neutron rate and fast-ion density ($\Delta S_n/S_n$ and $\Delta N_f/N_f$) after TAE avalanches. (b) Fractional losses vs variation in the maximum gradient (absolute value) at the low-field side after an avalanche. (c) Fractional losses vs variation in the position of the steepest gradient after an avalanche, showing an outward excursion associated with higher losses.

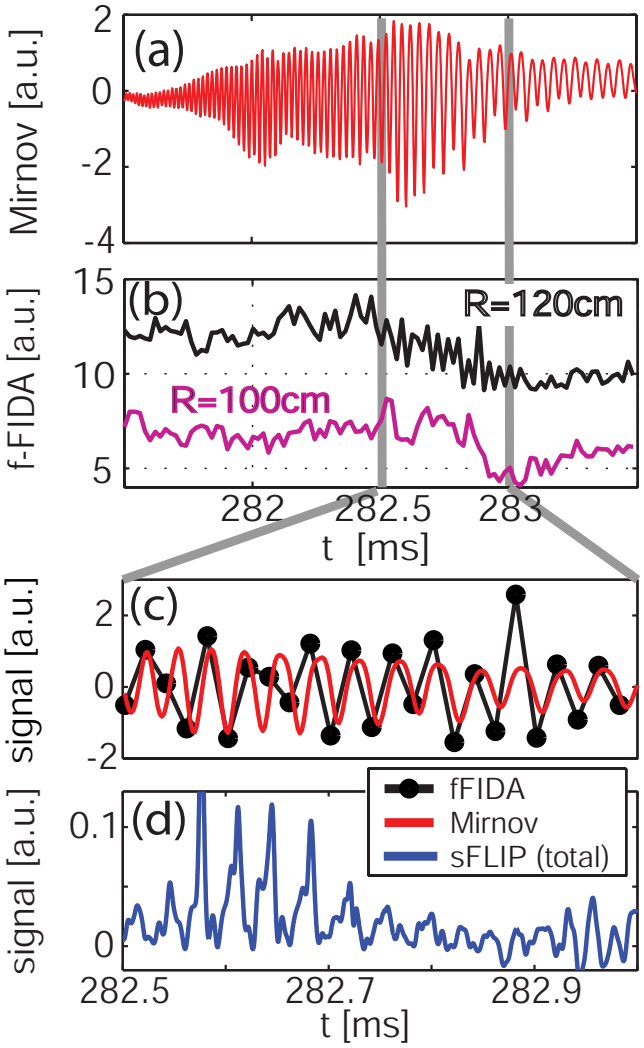


FIG. 10. (Color) [(a) and (b)] Signals from Mirnov coils, measuring frequency fluctuations ($f<200$ kHz), and the two f-FIDA channels ($R=100$ and 120 cm) during an avalanche for shot 128455. (c) Detail of the Mirnov and f-FIDA ($R=120$ cm) signals during the last phase of an avalanche. (c) Total signals from the sFLIP probe.

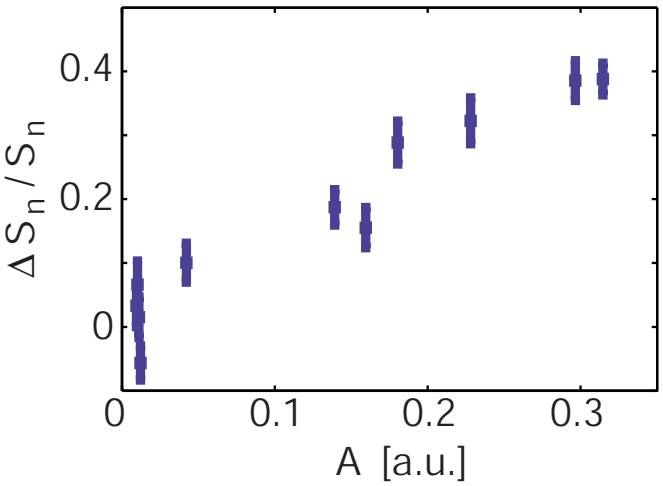


FIG. 11. (Color online) Fractional neutron rate drop vs amplitude of TAE modes during an avalanche as measured by Mirnov coils.

addition, the variation in the *position* of the steepest gradient is shown in Fig. 9(c). After an avalanche event, an outward shift of up to 5 cm is observed. Both effects, relaxation of the profile and outward shift of the steepest gradient location, are enhanced for larger losses. Moreover, it is observed that the radial gradient of $N_f$ steepens up in time *before* an avalanche occur. We conclude that the experimental results are consistent with an overall relaxation of the fast-ion profile *as a result* of the avalanche, which therefore leads to a decrease in the drive for the TAE precursors from which it originates.

Because the results illustrated so far are obtained with 10 ms temporal resolution, they are indicative of the overall effects of avalanches on fast ions. Information about the dynamics on time scales $\leq 100$ $\mu$s is gathered from the f-FIDA system, featuring a much higher temporal resolution than s-FIDA. An example is shown in Fig. 10, where the two channels at $R=100$ cm and $R=120$ cm are compared to the signal from magnetics coils and from the sFLIP probe. Interestingly, the drop in the f-FIDA traces is delayed with respect to that of the neutrons by about 0.4 and 0.9 ms for the channels at $R=120$ cm and $R=100$ cm, respectively. This may be indicative of a complex dynamics of $N_f$ on short time scales, with the outboard profile responding earlier than the inboard one to the perturbation. In fact, as the frequency of the dominant $n=2$ mode decreases to $\approx 25$ kHz, viz. the Nyquist frequency of the f-FIDA system, fluctuations become visible on the f-FIDA signal looking at $R=120$ cm [Fig. 10(a)]. The high correlation between signals from FIDA and Mirnov coils is shown in Fig. 10(b). A similar modulation is detected on the total sFLIP signal [Fig. 10(c)], which is proportional to fast-ion losses at the edge integrated over energy and pitch. Since the total sFLIP signal is sampled at 5 MHz, fluctuations associated with the other modes $n>2$ at higher frequency are also detected. The latter observations establish a link between behavior of the confined fast ions interacting with the instability and the corresponding loss from the confined plasma.

As a further step, the relationship between losses and TAE activity is investigated. Figure 11 illustrates the dependence of fractional losses upon amplitude of the modes, $A$, as calculated from Mirnov coils. $A$ is obtained by integrating the Mirnov signal over a 0.6 ms time window around the time of maximum activity. A clear trend is observed, with higher losses corresponding to larger signals. However, the comparison between $A$ calculated from Mirnov coils and from reflectometer data over multiple shots does not show a clear correspondence. The question about how to interpret the results in Fig. 11 is therefore still open. Two possible explanations are most likely. First, Mirnov coils sample $A$ at the edge of the plasma, in contrast to the reflectometer. Their response depends on the actual mode amplitude and on their spatial structure, with perturbations closer to the edge resulting in a larger signal. Second, the mode structure may evolve during an avalanche, making the response of Mirnov coils not necessarily proportional to that of the reflectometer channels over time. Both these issues reveal the necessity of knowing more in detail the mode structure and, in general, to have a reliable model for the observed features, as discussed in Sec. IV.

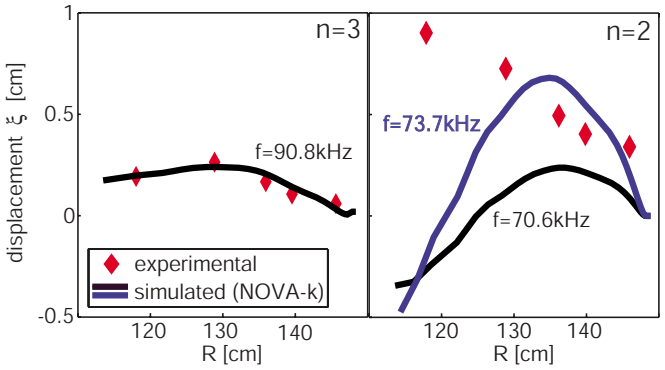


FIG. 12. (Color online) Comparison between the displacement $\xi$ measured by the reflectometer (symbols) and simulated by NOVA-k (solid lines) for the $n=3$ (left) and $n=2$ modes (right).

## IV. MODELING OF FAST-ION LOSSES BY TAE AVALANCHES

In this section the possibility of modeling the effects of the interaction between TAEs and fast ions is explored, with focus on the total loss following an avalanche. Fast-ion losses are modeled in three steps.[28] First, the equilibrium properties and the linear magnetohydrodynamics stability are calculated for the time at which the avalanche occurs through the TRANSP and NOVA-K codes.[29,30] Second, a selection is performed among all the possible unstable eigenmodes found by NOVA-K by comparing the mode structure measured by the multichannel reflectometer system with a synthetic output calculated from the simulation. Third, the selected eigenmodes are used in the ORBIT code[31] to simulate the fast-ion loss. To mimic the observed TAE behavior during an avalanche, the mode amplitude (frequency) can be modeled with a linear increase (decrease) as a function of time in ORBIT. The comparison between calculated and simulated eigenmodes is shown in Fig. 12 for the discharge illustrated in Fig. 7. In general, most of the unstable roots from NOVA-K have a global character, extending from the core out to the plasma edge. For the $n=3$ mode a good match is found for a specific eigenmode, whose frequency is compatible with the observed one, once the possible correction for the Doppler shift from plasma rotation is accounted for. However, no good solutions can be found for the dominant $n=2$ mode: the input eigenmodes to run the ORBIT code and calculate the total losses cannot be identified. The reason for the discrepancy between measurements and model must be identified to proceed with the comparison with theory. As a first possibility, we note that small variations in the $q(R)$ profile may result in a different structure of the Alfvén continuum, hence of the mode structure. Analysis performed with a shift of $q(R)$ of $\pm 0.1$, within the experimental uncertainties, is insufficient to reconcile the theory with the experiments. A second possibility, supported by the turbulent dynamics of the mode illustrated in Sec. III, is that a linear stability analysis cannot capture the actual mode structure. From previous analyses, a successful identification of the eigenmodes has been obtained for avalanches accompanied by fast-ion losses of 15%.[28] This may be explained by assuming that most of the losses during an avalanche are caused by nonlinear processes, and therefore the amount of losses is somewhat indicative of the degree of nonlinearity. In that case, a 40% loss in fast-ion population would imply that nonlinearities are too strong to be convincingly recovered through linear analysis. In particular, the procedure utilized herein does not treat self-consistently the possible evolution of plasma parameters, mode structure, and fast-ion distribution function during an avalanche. Numerical codes that can account for the three-dimensional, nonlinear dynamics with a self-consistent approach, such as the M3D code,[32] may be more appropriate to acquire better predictive capability on fast-ion transport caused by strongly nonlinear events.

## V. SUMMARY AND CONCLUSIONS

To summarize the results presented in this paper, it has been shown that TAE avalanches represent an efficient mechanism for fast-ion loss. Up to 40% of the fast-ion population can be expelled from the confined plasma after a single avalanche. According to theory and experimental results, a repetitive cycle of avalanches may be established for otherwise stationary plasma conditions. The resulting cumulative effect on the plasma performance can be rather dramatic. In order to extrapolate the results obtained on NSTX to other devices, two main aspects must be considered. First, TAEs on NSTX have a broad radial structure. On devices with higher toroidal field TAEs can be much more localized in space, and the losses may be replaced by a redistribution of fast ions inside the plasma volume. Second, the fast-ion distribution function in future fusion reactors will be substantially different from that originating from NB injection on NSTX due to the additional source of alpha particles.[33] This may have consequences on the destabilization of TAEs as well as on their dynamics. In any case, the impact of TAE avalanches on the dynamics of a future reactor, such as ITER, might represent a serious concern. A number of interlaced issues and open questions arise from the present work; the most urgent are the following.

(1) Are present-day experimental, theoretical, and numerical tools good enough to understand and model the observed behavior of TAE modes?
(2) Are we able to predict what the TAE behavior will be in future devices, such as ITER, and how can we mitigate (or, possibly, prevent) its negative impact for the performance of a fusion reactor?

Answers to point (1) are increasingly provided by experiments, developing improved tools to investigate fast-ion dynamics. For example, a coverage of the whole plasma region with different fast-ion diagnostics allows one to relate the behavior of confined fast particles with losses and underlying instabilities. At the same time, theory and simulations have shown dramatic improvements in the past years toward a global, nonlinear treatment of the plasma dynamics. The experimental results presented in this paper provide a challenging benchmark to test the capability of numerical simulations, following guidelines which are becoming widely accepted.[34] Among the others, features such as the strong modification of the fast-ion profile following an avalanche,

hence of the drive for TAEs, should be reproduced by numerical codes. Also, simulations may provide details on the fast-ion evolution on short time scales to be compared with experimental data, e.g., from the f-FIDA system and from the sFLIP probe. Answering point (2) requires a stronger effort in integrating experiments and theory to reach the required predictive capability.

## ACKNOWLEDGMENTS

The support of PPPL and NSTX team is gratefully acknowledged. This work is supported by U.S. DOE Grant No. DE-FG02-06ER54867 and by U.S. DOE Contract Nos. DE-AC02-76CH03073 and DE-FG02-99ER54527.

[1] W. W. Heidbrink, Phys. Plasmas **15**, 055501 (2008).
[2] F. Porcelli, Plasma Phys. Controlled Fusion **33**, 1601 (1991).
[3] R. B. White, E. D. Fredrickson, D. S. Darrow, M. Zarnstorff, R. Wilson, S. Zweben, K. Hill, Y. Chen, and G. Fu, Phys. Plasmas **2**, 2871 (1995).
[4] A. Fasoli, C. Gormezano, H. L. Berk, B. Breizman, S. Briguglio, D. S. Darrow, N. Gorelenkov, W. W. Heidbrink, A. Jaun, S. V. Konovalov, R. Nazikian, J.-M. Noterdaeme, S. Sharapov, K. Shinohara, D. Testa, K. Tobita, Y. Todo, G. Vlad, and F. Zonca, Nucl. Fusion **47**, S264 (2007).
[5] B. V. Chirikov, Phys. Rep. **52**, 263 (1979).
[6] H. L. Berk, B. N. Breizman, J. Fitzpatrick, M. S. Pekker, H. V. Wong, and K. L. Wong, Phys. Plasmas **3**, 1827 (1996).
[7] E. D. Fredrickson, N. N. Gorelenkov, R. E. Bell, J. E. Menard, A. L. Roquemore, S. Kubota, N. A. Crocker, and W. Peebles, Nucl. Fusion **46**, S926 (2006).
[8] M. Ono, S. M. Kaye, Y.-K. M. Peng, G. Barnes, W. Blanchard, M. D. Carter, J. Chrzanowski, L. Dudek, R. Ewig, D. Gates, R. E. Hatcher, T. Jarboe, S. C. Jardin, D. Johnson, R. Kaita, M. Kalish, C. E. Kessel, H. W. Kugel, R. Maingi, R. Majeski, J. Manickam, B. McCormack, J. Menard, D. Mueller, B. A. Nelson, B. E. Nelson, C. Neumeyer, G. Oliaro, F. Paoletti, R. Parsells, E. Perry, N. Pomphrey, S. Ramakrishnan, R. Raman, G. Rewoldt, J. Robinson, A. L. Roquemore, P. Ryan, S. Sabbagh, D. Swain, E. J. Synakowski, M. Viola, M. Williams, J. R. Wilson, and NSTX Team, Nucl. Fusion **40**, 557 (2000).
[9] S. S. Medley, N. N. Gorelenkov, R. Andre, R. E. Bell, D. S. Darrow, E. D. Fredrickson, S. M. Kaye, B. P. LeBlanc, A. L. Roquemore, and NSTX Team, Nucl. Fusion **44**, 1158 (2004).
[10] E. D. Fredrickson, R. E. Bell, D. S. Darrow, G. Fu, N. N. Gorelenkov, B. P. LeBlanc, S. S. Medley, J. E. Menard, H. Park, and A. L. Roquemore, Phys. Plasmas **13**, 056109 (2006).
[11] E. D. Fredrickson, C. Z. Cheng, D. S. Darrow, G. Fu, N. N. Gorelenkov, G. J. Kramer, S. S. Medley, J. E. Menard, and A. L. Roquemore, Phys. Plasmas **10**, 2852 (2003).
[12] N. N. Gorelenkov, H. L. Berk, and E. D. Fredrickson, S. E. Sharapov, Phys. Lett. A **370**, 70 (2007).
[13] N. N. Gorelenkov, H. L. Berk, N. A. Crocker, E. D. Fredrickson, S. M. Kaye, S. Kubota, H. Park, W. Peebles, S. A. Sabbagh, and S. E. Sharapov, Plasma Phys. Controlled Fusion **49**, B371 (2007).
[14] N. N. Gorelenkov, C. Z. Cheng, E. D. Fredrickson, E. Belova, D. Gates, S. M. Kaye, G. J. Kramer, R. Nazikian, and R. White, Nucl. Fusion **42**, 977 (2002).
[15] N. N. Gorelenkov, E. D. Fredrickson, E. Belova, C. Z. Cheng, D. Gates, S. M. Kaye, and R. White, Nucl. Fusion **43**, 228 (2003).
[16] W. W. Heidbrink, K. H. Burrell, Y. Luo, N. A. Pablant, and E. Ruskov, Plasma Phys. Controlled Fusion **46**, 1855 (2004).
[17] W. W. Heidbrink, Y. Luo, K. H. Burrell, R. W. Harvey, R. I. Pinsker, and E. Ruskov, Plasma Phys. Controlled Fusion **49**, 1457 (2007).
[18] M. Podestà, W. W. Heidbrink, R. E. Bell, and R. Feder, Rev. Sci. Instrum. **79**, 10E521 (2008).
[19] W. W. Heidbrink, R. E. Bell, Y. Luo, and W. Solomon, Rev. Sci. Instrum. **77**, 10F120 (2006).
[20] K. Shinohara, D. S. Darrow, A. L. Roquemore, S. S. Medley, and F. E. Cecil, Rev. Sci. Instrum. **75**, 3640 (2004).
[21] D. Liu, W. W. Heidbrink, D. S. Darrow, A. L. Roquemore, S. S. Medley, and K. Shinohara, Rev. Sci. Instrum. **77**, 10F113 (2006).
[22] S. S. Medley and A. L. Roquemore, Rev. Sci. Instrum. **75**, 3625 (2004).
[23] S. S. Medley, A. J. Donné, R. Kaita, A. I. Kislykov, M. P. Petrov, and A. L. Roquemore, Rev. Sci. Instrum. **79**, 011101 (2008).
[24] D. S. Darrow, Rev. Sci. Instrum. **79**, 023502 (2008).
[25] B. P. LeBlanc, R. E. Bell, D. W. Johnson, D. E. Hoffman, D. C. Long, and R. W. Palladino, Rev. Sci. Instrum. **74**, 1659 (2003).
[26] S. Kubota, W. A. Peebles, X. V. Nguyen, N. A. Crocker, and A. L. Roquemore, Rev. Sci. Instrum. **77**, 10E926 (2006).
[27] F. M. Levinton, R. J. Fonck, G. M. Gammel, R. Kaita, H. W. Kugel, E. T. Powell, and D. W. Roberts, Phys. Rev. Lett. **63**, 2060 (1989).
[28] E. D. Fredrickson, Bull. Am. Phys. Soc. **53**(14), 189 (2008).
[29] R. V. Budny, Nucl. Fusion **34**, 1247 (1994).
[30] C. Z. Cheng, Phys. Rep. **211**, 1 (1992).
[31] R. B. White and M. S. Chance, Phys. Fluids **27**, 2455 (1984).
[32] W. Park, E. V. Belova, G. Fu, X. Z. Tang, H. R. Strauss, and L. E. Sugiyama, Phys. Plasmas **6**, 1796 (1999).
[33] W. W. Heidbrink, Phys. Plasmas **9**, 2113 (2002).
[34] P. W. Terry, M. Greenwald, J.-N. Leboeuf, G. R. McKee, D. R. Mikkelsen, W. M. Nevins, D. E. Newman, D. P. Stotler, Task Group on Verification and Validation, U.S. Burning Plasma Organization, and U.S. Transport Task Force, Phys. Plasmas **15**, 062503 (2008).